Temperature and Final State Effects in Radio Frequency Spectroscopy Experiments on Atomic Fermi Gases

Yan He, Chih-Chun Chien, Qijin Chen, and K. Levin

James Franck Institute and Department of Physics, University of Chicago, Chicago, Illinois 60637, USA

(Received 9 April 2008; published 14 January 2009)

We present a simple and systematic characterization of the radio frequency (rf) spectra of homogeneous, paired atomic Fermi gases at general temperatures T in the presence of final-state interactions. The spectra, consisting of possible bound states and positive as well as negative detuning (ν) continua, satisfy exactly the zeroth- and first-moment sum rules at all T. We show how to best extract the pairing gap and how to detect the $\nu < 0$ continuum arising from thermally excited quasiparticles, not yet seen experimentally. We explain semiquantitatively recent rf experiments on ''bound-bound'' transitions, predicting effects of varying temperature.

DOI: 10.1103/PhysRevLett.102.020402 PACS numbers: 03.75.Hh, 03.75.Ss, 74.20.−z

The superfluid and normal phases in trapped Fermi gases undergoing BCS to BEC crossover have presented us with novel forms of superfluidity. An important characteristic of any superfluid is the pairing gap which is best probed in the gases using radio frequency (rf) spectroscopy. This technique has been addressed experimentally [1–3] as well as theoretically [4–9]. The goal of this paper is to present a single formalism for the rf spectra at all T and all frequencies, including the final-state effects [6–9]. Armed with a full understanding, we show how to extract the gap $\Delta(T)$. By including the effects of finite T, not only does this lead to a better experimental insight into the entire spectrum, but it provides a basis for comparing and assessing different theoretical approaches to BCS-BEC crossover.

A successful theory of a Fermi gas near unitarity not only has a pairing gap which appears [4,5,7] at $T^* > T_c$, but also (i) exhibits a second order phase transition at T_c. Studies of this smoothly varying (from above T^* to $T = 0$) pairing gap, reminiscent of its counterpart in the high T_c superconductors, may elucidate some of the physics of the cuprates [10]. (ii) On physical grounds [4,5,7] it is clear that the rf current $I(\nu)$ reflects the pairing gap $\Delta(T)$ rather than coherent superfluid order parameter $\Delta_{sc}(T)$. At odds with this first observation is the fact that all crossover theories which include pairing fluctuations [11–14] except the present one, lead to first order transitions at T_c. At odds with the second observation is that alternative calculations [8,9,15] of $I(\nu)$ consider only the $T \approx 0$ superfluid and/or separately the normal phase even though, at $T < T^*$, the presence or absence of superfluid order in the rf spectra should not lead to fundamentally different physics.

We consider a homogeneous system, relevant to recent tomographic experiments [2]. We find at $T \neq 0$, the spectrum consists of (possibly) bound state contributions which either appear at positive or negative detuning, ν and, (always), positive as well as negative ν continuum contributions which reflect Δ and the fermionic chemical potential μ. We emphasize the $\nu < 0$ continuum which derives from thermally excited quasiparticles, first discussed in Ref. [16]. A central finding is that it can be strongly enhanced by final-state interactions and made visible in future tomographic experiments. Near unitarity, these bound state enhancements of the $\nu < 0$ continuum facilitate the extraction (using sum rules) of the gap Δ and the chemical potential μ. We explain semiquantitatively recent low T experiments and make predictions for the accompanying T dependences which should be observable.

The rf technique focuses on the three lowest energy atomic hyperfine states (two of which are involved in the pairing, while a third provides a final ''excited'' state for one component of a pair). For definiteness, we first consider a superfluid of pairs in the equally populated hyperfine 1–2 levels and apply a radio frequency ω_{23} to excite the atoms in state 2 to state 3. Based on linear response, [4–6] our T-matrix-based formulation of the finite T rf problem is compatible (in the $T \to 0$ limit) with that of Refs. [8,9].

The T-matrix used here (for the 1–2 channel) is consistent [10,17] with the BCS-Leggett ground state equations and involves one bare and one dressed Green's function in the form

$$t_{12}^{-1}(Q) = g_{12}^{-1} + \sum_K G_1(K) G_2^0(Q - K), \tag{1}$$

$$t_{13}^{-1}(Q) = g_{13}^{-1} + \sum_K G_1(K) G_3^0(Q - K), \tag{2}$$

where g_{12} and g_{13} parameterize the interaction between 1 and 2 and 1 and 3, respectively. We have introduced the dressed Green's function $G = [(G^0)^{-1} - \Sigma]^{-1}$ and G^0 is the Green's function of the noninteracting system. Here the subscripts indicate the hyperfine levels, $K \equiv (i\omega_l, \mathbf{k})$, $Q \equiv (i\Omega_n, \mathbf{q})$ are 4-momenta with $\sum_K \equiv T\sum_l \sum_{\mathbf{k}}$, etc., and ω_l and Ω_n are fermion and boson Matsubara frequencies, respectively. Throughout we take $\hbar = k_B = 1$ and assume a contact potential (so that the strict Hartree self-energy vanishes) and a (nearly) empty population in the hyperfine 3 state so that $G_3(K) \approx G_3^0(K)$. As has been demonstrated elsewhere [10], it is reasonable to take the self-energy (on

the real frequency axis) in the Green's functions G_1 and G_2 to be of the generalized BCS form $\Sigma(\omega, \mathbf{k}) \approx \frac{\Delta^2}{\omega+\epsilon_{\mathbf{k}}}$ although this approximation is not essential. Similarly, we have shown [10] that, below T_c, $\Delta(T)$ is constrained by a BCS-like gap equation which can be written as $1 + g_{12}\chi_{12}(0) = 0$ where $\chi_{12}(Q) = \sum_K G_1(K)G_2^0(Q - K)$, in conjunction with a fermion number equation. More generally, the propagator for noncondensed pairs is of the form $t_{12}(Q) = g_{12}/[1 + g_{12}\chi_{12}(Q)]$.

In this way, one derives the usual gap (determining $\Delta(T)$) and number [determining $\mu(T)$] equations associated with generalized BCS theory. The difference between the excitation gap $\Delta(T)$ and the order parameter $\Delta_{\rm sc}(T)$ is associated [10] with noncondensed pair effects parameterized by $\Delta_{\rm pg}^2$, which enter as

$$\Delta_{\rm pg}^2(T) = \Delta^2(T) - \Delta_{\rm sc}^2(T) = -\sum_{Q\neq 0} t_{12}(Q). \tag{3}$$

Thus, the pseudogap, $\Delta_{\rm pg}$, persisting above T_c is self consistently determined and T_c is deduced [10] as the T where $\Delta_{\rm sc}(T)$ first vanishes. We find $T_c = 0.25T_F$ at unitarity.

The resulting diagram set for the rf response function, $D(Q)$, which depends on $\Delta(T)$ is shown in Fig. 1. It is convenient notationally to define a form of Gor'kov F function in terms of the pairing gap as $\Delta G_2(K)G_1^0(-K) = \Delta/(\omega_l^2 + E_k^2) \equiv F(K)$ where $E_k = \sqrt{\xi_k^2 + \Delta^2(T)}$, and $\xi_k = \epsilon_k - \mu$, $\epsilon_k = k^2/2m$. The first term on the right or leading order term, $D_0(Q)$, of the response function appears as the bubble and was introduced in Ref. [4]. It is given by $D_0(Q) = \sum_K G_2(K)G_3^0(K + Q)$. From this we can write the current (without final-state effects) as $I_0(\nu) = -(1/\pi)\mathrm{Im}D_0^R(\Omega)$. The second term on the right corresponds to the Aslamazov-Larkin (AL) diagram [17] (called $D_{\rm AL}$) which incorporates final-state effects. We neglect the effects arising from the interaction between 2 and 3, as in the approach in Ref. [6].

Because of the constraints imposed by the BCS-like gap equation, $t_{12}(Q)$ diverges at $Q = 0$ so that it is reasonable to set Q in t_{12} to zero, i.e., $t_{12}(Q) \approx -(\Delta^2/T)\delta(Q)$. This assumption, leading to the approximated form for $\Sigma(\omega, \mathbf{k})$, is not essential for understanding the physics but it does greatly simplify the calculations [18]. For this reason we

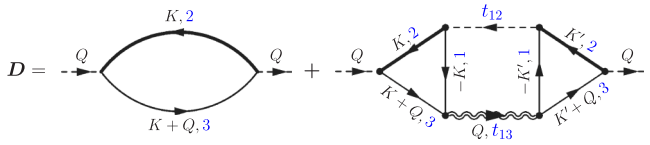

FIG. 1 (color online). Feynman diagrams for the rf response function $D(Q)$. The left bubble is the lowest order D_0, whereas the right diagram, $D_{\rm AL}$, is associated with final-state effects. Here thin (thick) lines stand for bare (full) fermion propagators, the dashed line for t_{12}, approximated as the condensate, and double wiggly line for t_{13}. The numbers in blue indicate the hyperfine levels.

adopt the counterpart assumption for evaluating $D_{\rm AL}$ in Fig. 1 which corresponds to introducing opposite momenta $\pm K$ for particles 1 and 2 in this diagram.

Writing out the AL diagram yields $D_{\rm AL}(Q) = [\sum_K F(K)G_3^0(K + Q)]^2 t_{13}(Q)$. For the rf field, $Q = (i\Omega_n, \mathbf{0})$ so that $D(i\Omega_n) \equiv D(Q)$. We take μ_3 satisfying $f(\xi_{k,3}) = 0$, where $\xi_{k,3} = \epsilon_k - \mu_3$. Then the rf current, given by the retarded response function, is $I(\nu) \equiv -(1/\pi)\mathrm{Im}D^R(\Omega)$, where $\Omega \equiv \nu + \mu - \mu_3$, and

$$D(Q) = D_0(Q) + \frac{[D_2(Q)]^2}{m/4\pi a_{13} + D_1(Q)}. \tag{4}$$

Here $D_2(Q) \equiv \sum_K F(K)G_3^0(K + Q)$ and $D_1(Q) \equiv \sum_K G_1(K)G_3^0(Q - K) - \sum_{\mathbf{k}}(1/2\epsilon_k)$. We note that $t_{13}^{-1}(Q) = m/4\pi a_{13} + D_1(Q)$, where a_{13} (and a_{12}) are the s-wave scattering length in the 1–3 (and 1–2) channels, respectively. In general, features in the rf spectra derive from the poles and imaginary parts of $D_0(Q)$, $D_1(Q)$ and $D_2(Q)$. We note that these three complex functions are the same as their wave function calculation counterparts [9] if the pairing gap Δ is chosen to be order parameter $\Delta_{\rm sc}$ and $T \equiv 0$. It is ν not Ω that should be identified with the experimental rf detuning. Here and below, we make use of the fact that we can write

$$t_{13}^{-1}(0) = (g_{13}^{-1} - g_{12}^{-1}) + t_{12}^{-1}(0) = g_{13}^{-1} - g_{12}^{-1}. \tag{5}$$

This leads to the central analytical result of this Letter, which shows, how with final-state effects included, the rf current can be written in a very compact and simple form

$$\begin{aligned} I(\nu) &= \left[\frac{1}{g_{12}} - \frac{1}{g_{13}}\right]^2 \frac{I_0(\nu)}{|\bar{t}_{13}^{-1,R}(\nu)|^2} \\ &= -\frac{1}{\pi}\left[\frac{m}{4\pi a_{13}} - \frac{m}{4\pi a_{12}}\right]^2 \frac{\Delta^2}{\nu^2}\,\mathrm{Im}\bar{t}_{13}^R(\nu), \end{aligned} \tag{6}$$

where $\bar{t}_{13}^R(\nu) \equiv t_{13}^R(\Omega)$. This expression can be readily extended to include the effects of population imbalance. The simplicity of this result, which is built around strict BCS mean field theory (except that $\Delta(T) \neq \Delta_{\rm sc}(T)$), should make it accessible for general application, without requiring complicated numerics. The calculations are no more complex than those for $I_0(\nu) = (1/\pi) \times (\Delta^2/\nu^2)\mathrm{Im}\bar{t}_{13}^{-1,R}(\nu)$, since one generally calculates $\mathrm{Re}\bar{t}_{13}^{-1,R}(\nu)$ as well. Note that after some straightforward algebra, one can show that when $g_{13} = g_{12}$ there is an exact cancellation such that $I(\nu) \sim \delta(\nu)$.

Equations (6) make it clear that final-state effects in the rf current directly reflect the T matrix in the 1–3 channel. Thus, the spectrum may contain a bound state associated with poles at ν_0 in t_{13}, as determined by $t_{13}^{-1}(\nu_0) = 0$. This leads to the so-called "bound-bound" transition. In addition, there is a continuum associated with both the numerator and denominator in the first of Eqs. (6), with each contribution spanned by the limits of $\nu = \xi_k \pm E_k$, i.e., $-(\sqrt{\mu^2 + \Delta^2} + \mu) \leq \nu \leq 0$ and $\nu \geq \sqrt{\mu^2 + \Delta^2} - \mu$.

The continuum at positive frequencies is primarily associated with breaking a pair and promoting the state 2 to state 3. This represents the so-called "bound-free" transition. On the negative detuning side, the continuum is primarily associated with promoting to state 3 an already existing thermally excited 2 particle. The spectral weight of the negative continuum vanishes exponentially at low T as $e^{-\Delta/T}$. Therefore, there is a strong asymmetry in the continuum with the bulk of the weight on the positive frequency side for low T. If the bound state falls within the negative continuum, it will acquire a finite lifetime, and decay quickly at high T.

Of importance, in assessing a theoretical framework for computing the rf current are the two sum rules associated with the total integrated current and the first moment or "clock shift" [6]. Using the Kramers-Kronig relations between $\mathrm{Re}t_{13}^R$ and $\mathrm{Im}t_{13}^R$, it is easy to prove that, not only in the ground state, but also at finite temperature, Eq. (6) satisfies $\int d\nu I(\nu) = n_2 - n_3$ and $\int d\nu \nu I(\nu) = \Delta^2 \frac{m}{4\pi}(\frac{1}{a_{12}} - \frac{1}{a_{13}})$ where n_2 and $n_3(=0)$ are the density of state 2 and 3 atoms, respectively. Then the clock shift is

$$\bar{\nu} = \frac{\int d\nu \nu I(\nu)}{\int d\nu I(\nu)} = \frac{\Delta^2}{n_2 - n_3} \frac{m}{4\pi}\left(\frac{1}{a_{12}} - \frac{1}{a_{13}}\right), \qquad (7)$$

which agrees with Ref. [6] when $n_3 \to 0$. This sum rule is satisfied only when $a_{13} \neq 0$ and when both diagrammatic contributions are included. It is easy to show that at large ν, $I_0(\nu) \sim \nu^{-3/2}$, $\mathrm{Im}t_{13}^R \sim \nu^{-1/2}$, so that $I(\nu) \sim \nu^{-5/2}$, in agreement with Ref. [8]. Clearly, the first moment of $I(\nu)$ is integrable, whereas the first moment of $I_0(\nu)$ is not. Finally, Eq. (6) reveals that the spectral weight (including possible bound states) away from $\nu = 0$ will disappear when the gap Δ vanishes.

Figures 2(a) and 2(b) illustrate the behavior of the spectrum $I(\nu)$ when the initial state 1–2 pairing is at unitarity (i.e., at 834 G) and the final-state 1–3 pairing is on the BCS side of the 1–3 resonance, for temperatures $T/T_F = 0.1$, 0.3, and 0.45. The parameters we use are taken from Ref. [19]. The inset of Fig. 2(a) indicates the behavior in the absence of final-state effects for the same temperatures. The asymmetry of the continuum around $\nu = 0$, discussed earlier, is evident even in this leading order bubble diagram. As T is raised the spectrum becomes more symmetric. In Fig. 2(a), the final-state interaction $1/k_F a_{13} = -1$ is relatively weak, and there is no bound state. In contrast, at $1/k_F a_{13} = -0.5$ (or $T_F \approx 6\ \mu$K) in Fig. 2(b), a bound state emerges at low T (although it disappears at moderate temperatures when the gap becomes small). For the low $T_F \sim 2.5\ \mu$K used in Ref. [1], and taking $1/k_F a_{13} = -0.77$ from the literature [19], we do not find a bound state. These results are consistent with $T = 0$ calculations of Basu and Mueller [9]. It should be stressed that, at 834 G for a typical T_F, when the bound-bound transition occurs, it is barely separated from the asymmetric bound-free continuum, which is always present.

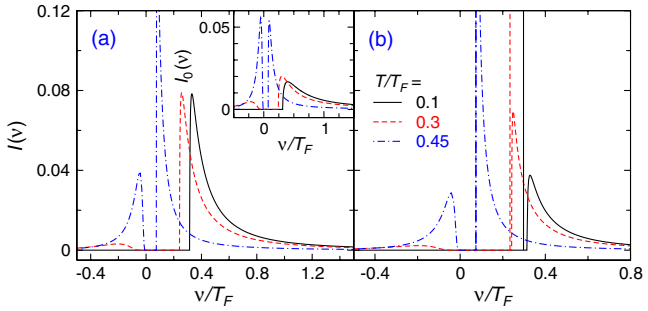

FIG. 2 (color online). rf current $I(\nu)$ as a function of rf detuning ν for transitions from unitarity $1/k_F a_{12} = 0$ at 834 G to final state (a) $1/k_F a_{13} = -1$ and (b) -0.5 in the BCS regime, corresponding to $T_F = 31$ and 124 kHz, respectively. The temperatures are $T/T_F = 0.1$ (black solid), 0.3 (red dashed) and 0.45 (blue dot-dashed lines). Here $T_c = 0.25 T_F$. The sharp lines next to the right continuum in (b) correspond to bound states. Inset: Lowest order rf current $I_0(\nu)$ vs ν.

Figure 3 presents the analogous plots at different T for rf transitions from an initial 1–3 superfluid with $T_F =$ 40 kHz at (a) 811 and (b) 750 G, which are on the BCS side of the 1–3 resonance (which appears at 690 G). The system is subject to an rf field promoting state 1 to state 2. "Bound-bound-like transitions" [20] now appear. In Fig. 3(a), the bound state falls within the negative detuning continuum. Importantly, the disappearance of the bound state with temperature is preceded by a very unusual two-peaked spectrum in the negative detuning regime, which is seen at the two higher T. We can understand this unusual structure as a combination of the peak from the negative continuum which appears very close to $\nu = 0$, (as also seen in Fig. 2) and the nearby bound state peak. At even higher T, the spectral weight will shift almost completely to the region near $\nu = 0^-$ and the bound state decays rapidly. As $\nu \to 0^-$, the negative continuum peak is a combined effect of the vanishing $\mathrm{Im}\tilde{t}_{13}^R$ and the diverging factor $1/\nu^2$ in Eq. (6). In Fig. 3(b), the bound state is outside the con-

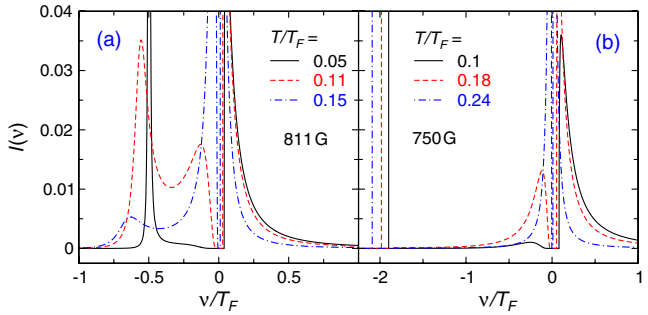

FIG. 3 (color online). rf current $I(\nu)$ as a function of detuning ν for $1 \to 2$ transitions in a 1–3 superfluid of $T_F = 40$ kHz (a) from $1/k_F a_{13} = -0.804$ to final states $1/k_F a_{23} = 0$ at 811 G, and (b) from $1/k_F a_{13} = -0.524$ to $1/k_F a_{23} = 0.68$ at 750 G, for different temperatures as labeled. Here $T_c/T_F = 0.15$ and 0.17, respectively. In (b) when T is high and Δ is small, the two peaks around $\nu = 0$ may not be resolvable experimentally.

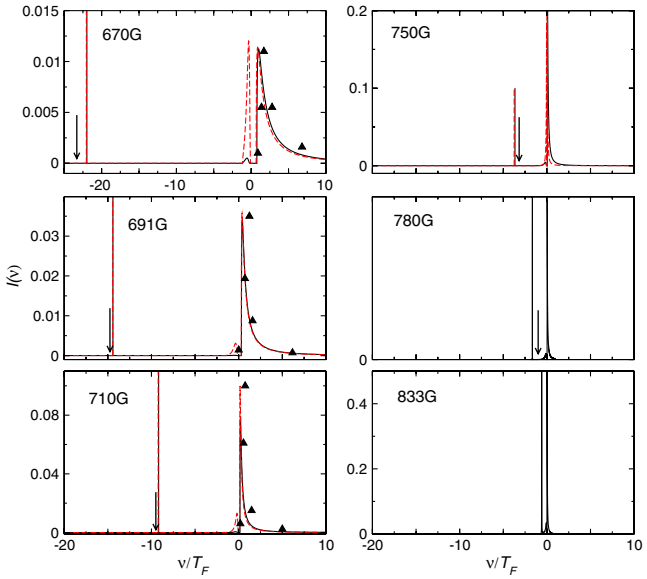

FIG. 4 (color online). rf current $I(\nu)$ as a function of detuning ν for a 1–3 superfluid with rf excitation from state 3 to state 2. The black curves are calculated at experimental parameters of $(1/k_F a_{13}, 1/k_F a_{12}, T/T_F) = (0.4, 3.3, 0.2)$, $(0.0, 2.6, 0.1)$, $(-0.3, 2.0, 0.1)$, $(-0.7, 1.1, 0.09)$, $(-0.9, 0.6, 0.09)$, and $(-1.2, 0.0, 0.06)$ from low to high fields. The red dashed curves are calculated at twice the temperatures. The sharp lines on the left indicate bound states. For comparison, experimental data are marked by arrows for bound peak locations and by triangles for the continuum.

tinuum, and the binding energy is fairly insensitive to temperature. We have chosen experimentally accessible parameters here, so that the unusual double-peaked structure in $I(\nu)$ at $\nu < 0$ should be observable. Finally, we emphasize that the highest T cases in Figs. 2 and 3 are at or above T_c, so that the continuum appears only because there exists a pseudogap in the fermionic spectrum.

Figure 4 addresses recent data [2] associated with 1–3 pairing and rf excitation from state 3 to state 2. The calculations of $I(\nu)$ shown in the (black) solid curves in all six panels were performed with experimental parameters, and should be compared with Fig. 4 of Ref. [2]. To help in the comparison a number of data points (normalized to the same peak height) have been inserted. The sharp bound states will, in the data, be broadened both instrumentally and from limited spatial and energy resolution. Except for a slight broadening which we have ignored here, our calculated black solid curves, which incorporate final-state effects, can be seen to be in semiquantitative agreement with experiment. We anticipate that at higher T (red dashed lines), the negative ν continuum states should start to become apparent. If seen, this will add further support for the present calculations, in addition to the reasonable, *a posteriori* agreement shown here.

Finally, we note that the most practical way to extract the pairing gap $\Delta(T)$ near unitarity, within the BCS-Leggett crossover formalism, is using the sum rule in Eq. (7). If one integrates the precise theoretical values in Fig. 3(a) (without any experimental broadening) from $\nu = -2T_F$ to $\nu = +2T_F$, the accuracy is within $\approx 20\%$. We find the accuracy is improved if one exploits final-state effects to create a bound state in the negative continuum as in Fig. 3(a). These observations lend underlying support to the importance of the present calculations and point out that future experiments should not focus exclusively on situations where final-state effects can be neglected. Finally, we note that, together with the $\nu > 0$ continuum threshold which appears at $\sqrt{\Delta^2 + \mu^2} - \mu$, one can also determine μ and hence the important factor β.

This work is supported by Grants NSF PHY-0555325 and NSF-MRSEC DMR-0213745. We thank S. Basu, C. Chin, S. Jochim, and E. Mueller for helpful discussions.

[1] C. Chin, M. Bartenstein, A. Altmeyer, S. Riedl, S. Jochim, J. H. Denschlag, and R. Grimm, Science **305**, 1128 (2004).
[2] C. Schunck, Y.-I. Shin, A. Schirotzek, and W. Ketterle, Nature (London) **454**, 739 (2008).
[3] C. H. Schunck, Y. Shin, A. Schirotzek, M. W. Zwierlein, and W. Ketterle, Science **316**, 867 (2007).
[4] J. Kinnunen, M. Rodriguez, and P. Törmä, Science **305**, 1131 (2004).
[5] Y. He, Q. J. Chen, and K. Levin, Phys. Rev. A **72**, 011602 (R) (2005); Y. He, C. C. Chien, Q. J. Chen, and K. Levin, Phys. Rev. A **77**, 011602(R) (2008).
[6] Z. Yu and G. Baym, Phys. Rev. A **73**, 063601 (2006); G. Baym, C. J. Pethick, Z. Yu, and M. W. Zwierlein, Phys. Rev. Lett. **99**, 190407 (2007).
[7] M. Punk and W. Zwerger, Phys. Rev. Lett. **99**, 170404 (2007).
[8] A. Perali, P. Pieri, and G. C. Strinati, Phys. Rev. Lett. **100**, 010402 (2008).
[9] S. Basu and E. J. Mueller, Phys. Rev. Lett. **101**, 060405 (2008).
[10] Q. J. Chen, J. Stajic, S. N. Tan, and K. Levin, Phys. Rep. **412**, 1 (2005).
[11] R. Haussmann, W. Rantner, S. Cerrito, and W. Zwerger, Phys. Rev. A **75**, 023610 (2007).
[12] P. Pieri, L. Pisani, and G. C. Strinati, Phys. Rev. B **70**, 094508 (2004).
[13] N. Fukushima, Y. Ohashi, E. Taylor, and A. Griffin, Phys. Rev. A **75**, 033609 (2007).
[14] H. Hu, P. D. Drummond, and X. J. Liu, Nature Phys. **3**, 469 (2007).
[15] P. Massignan, G. M. Bruun, and H. T. C. Stoof, Phys. Rev. A **77**, 031601(R) (2008).
[16] J. Kinnunen, M. Rodriguez, and P. Törmä, Phys. Rev. Lett. **92**, 230403 (2004).
[17] Q. J. Chen, I. Kosztin, B. Jankó, and K. Levin, Phys. Rev. Lett. **81**, 4708 (1998).
[18] Here we extend this approximation above the actual T_c as well, to estimate Δ and μ.
[19] M. Bartenstein *et al.*, Phys. Rev. Lett. **94**, 103201 (2005).
[20] C. Chin and P. S. Julienne, Phys. Rev. A **71**, 012713 (2005).